Final version is available on: https://doi.org/10.1016/j.envres.2020.110577

Strategic Design of Wall Envelopes for the Enhancement of Building Thermal Performance at Reduced Air-Conditioning Costs

Shaik Saboor[a], Arumugam Chelliah [a], Kiran Kumar Gorantla[b], Ki-Hyun Kim[c*], S-H. Lee[d], Zang Ho Shon[e], Richard J. C. Brown[f],

[a]Department of Thermal and Energy, Vellore Institute of Technology, Vellore-632014, Tamilnadu, India.[b] Department of Mechanical Engineering, Sasi Institute of Technology and Engineering Tadepalligudem-534101, Andhra Pradesh, India. [c]Department of Civil & Environmental Engineering, Hanyang University, 222 Wangsimni-Ro, Seoul 133-791, Republic of Korea,[d] Department of Environmental Science, Keimyung University, 1095 Dalgubeol-Daero, Daegu, 42601, Republic of Korea; [e]Department of Environmental Engineering, Dong-Eui University, Busan, Republic of Korea; [f]Environment Department, National Physical Laboratory, Teddington, TW11 0LW, UK

Abstract

A strategy is proposed for the design of wall envelopes to improve unsteady thermal performance parameters in non-air-conditioned buildings and to reduce energy costs in air-conditioned buildings. The thermophysical properties of building materials (e.g., burnt bricks, mud bricks, laterite stone, cinder concrete, and expanded polystyrene) were measured experimentally using a thermal analyzer. The total of 28 combinations of composite walls were designed with expanded polystyrene as an insulation material based on seven criteria and were subjected to 8 different external surface heat transfer coefficient, which were tested for unsteady thermal performance parameters and air-conditioning cost-saving potential. In this paper, unsteady thermal transmittance obtained from admittance method has been employed to compute cost saving potential of air-conditioning for the various wall envelopes. The use of C-H_5 design at a 2 m/s wind speed increases the decrement lag of burnt brick, mud brick, laterite stone, and cinder concrete composite wall envelopes by 48.1%, 49.0%, 59.5%, and 47.0%, respectively, relative to the common wall design (C-H_1) in non-air-conditioned buildings. The laterite with a C-H_5 design offers the highest annual energy cost savings (1.71 \$/m^2 at 2 m/s), highest life cycle cost savings (18.32 \$/m^2 at 2m/s), and the lowest payback period (4.03 yrs at 2 m/s) as compared to the other building materials in air-conditioned buildings. The overall results of this study are expected to open new paths to simple design considerations for energy-efficient buildings.

Keywords: Energy-efficient wall design; Attenuation factor; Decrement lag; Annual energy; Life cycle

*Correspondence: kkim61@hanyang.ac.kr

1. Introduction

Building materials serve as thermal mass in passive building designs. Heat transfer takes place at the air and building wall interface by both radiation and convection. The convective heat transfer at the air and building wall interface depends on convective heat transfer coefficients. These coefficients are adversely influenced by the atmospheric wind velocity; hence, the stability of the thermal characteristics of building walls is affected by changes in the atmospheric wind velocity (Davies, 2004).

The amplitude of the sinusoidal heatwaves decreases as they penetrate through a building envelope. This reduction is due to the thermal mass of the building material used for the envelope. The shrinkage of the heatwave from the outside to the inside of the building envelope is known as the attenuation factor. The time taken for the heat sine wave to penetrate through the building envelope is known as decrement delay (Duffin, 1984). Building enclosure materials should have low attenuation factors and high phase shift values to maintain comfortable indoor conditions (ASHRAE, 2001). Consequently, much effort has been made to evaluate the influence of building enclosure thickness and insulation location (e.g., within the enclosure) on variables such as phase lag or thermal delay and attenuation factor using the Crank–Nicolson (C-N) procedure (Antonopoulos and Koronaki, 2000; Lee Ok et al., 2014). The admittance method has been used to find the surface factor of building enclosures (Evola and Marletta, 2013), and can be used to assess the thermal characteristics of roofs and wall envelopes (Hall

M R, 2010; Najim, 2014; Najim and Fadhil, 2015; Shaik and Talanki, 2016). The effect of the thermophysical properties of wall enclosures on the decrement delay and attenuation factor has also been explored (Asan, H., 1998; Kontoleon et al., 2013; Ulgen, 2002). Atmospheric moisture and temperature can also affect the attenuation factor and decrement delay of laterite building wall enclosures (Shaik and Talanki Puttaranga Setty, 2016). A study of south-facing walls in the Mediterranean region indicated that a 0.2 increase in solar absorptivity increases the decrement delay; however, further increases in solar absorptivity decreased decrement delay (Kontoleon and Eumorfopoulou, 2008). The implicit finite difference procedure was adopted to compute attenuation factors and attenuation delays in Turkey (Ozel and Pihtili, 2007). The admittance method was customized to incorporate moisture-dependent unsteady parameters (Hall and Allinson, 2008). The attenuation factor and decrement delay of AAC concrete were studied (Ng et al., 2011), showing an increase in the thermal diffusivity of the wall enclosure materials increased the attenuation factor and decreased the decrement delay. Decrement delay and attenuation factor values have been computed by explicit control volume discretization (Mavromatidis et al., 2012) and the finite difference method. It has been suggested that decrement delay values could be affected by the azimuth angle of the wall enclosure (Ruivo et al., 2013). Moreover, a coconut fiber-filled, Ferro-cement prototype house was also found to offer higher resistance to heat flow at peak times compared to concrete slab roofing in Mexico (Alavez-Ramirez et al., 2014). Thermal performance studies of ventilated roofs showed that the best performance could be obtained by placing insulation close to the cold surface and below the air space layer (Gagliano et al., 2012). Various building envelope configurations were investigated for thermal performance using finite difference and admittance methods (Balaji et al., 2019). Expanded polystyrene was reported to be the best insulating material with a maximum life cycle cost savings and minimum payback period (Yu et al., 2009). A thermoeconomic method of optimizing the insulation thickness gave better results compared to the entransy-based environmental method (Gülten, 2020). The thickness of phase change materials and the insulation layer were simulated and optimized with simulation tools and generic algorithms (Baniassadi et al., 2016). It was concluded that the insulation layer is more effective than the phase change materials in moderate climates. The mathematical model for evaluating the economic and life cycle cost savings of insulation in the non-homogenous building walls was developed and studied (Huang et al., 2020). The Lagrangian optimization method was used to optimize the insulation thickness with the maximum life cycle cost savings and minimum payback period (Feng et al., 2018). The exergo-economic method was carried out to optimize the insulation thickness in a method where combustion parameters and insulation cost are considered (Arslan et al., 2010).

Currently, there is little information on the design of wall envelopes to reduce heat gain by convection and various wall design energies and cost assessments – especially considering low-cost building options in emerging economies. In this respect, we investigated the optimum design conditions for building wall envelopes to facilitate comfortable indoor conditions in hot climatic environments based on the thermal performance parameters of the walls. The thermal parameters considered in this study included: admittance, unsteady transmittance, attenuation factor, and decrement delay. The energy-economic parameters studied include annual energy cost savings, life cycle cost savings, and payback periods. The building envelope is a heat flow control element for the building. The appropriate design of the envelope reduces the building cooling loads. Heat transfer from the outer to the inner layer of the envelope depends mainly on the outside surface heat transfer coefficients. Therefore, in this paper, we proposed optimum envelope designs for reduced cooling loads under various external heat transfer coefficients. The reliability of the results has been validated against the Charted Institution of Building Services Engineers guide (CIBSE, 2006).

2. Materials and methodology

2.1 Materials

This study considered the most widely used building materials in India (i.e., burnt brick, mud brick, laterite stone, and cinder concrete). Burnt bricks are composed of clay (20-30% by mass), silt (20-35% by mass), and sand (35-50% by mass) (IS: 2117, 2002). The total content of clay, silt, and water should not be less than 50%. The molded bricks are fired in a kiln at temperatures ranging from 900-1000^{o}C to obtain burnt bricks. The compressive strength of burnt bricks should not be less than 3.5 N/mm^2 as per Indian standards. Mud bricks or adobe are made of clay (15% by mass), silt (10-30% by mass), and sand (50-70% by mass) mixed with straw, and they are air-dried before use. The compressive strength of mud bricks should not be less than 2 N/mm^2 for building applications as per Indian standard IS: 1725-1982 (IS: 1725, 1982). Laterite stone is abundantly available on the south-west coast of India. It is a readily available, eco-friendly, economical, and ferruginous building material. The compressive strength of laterite stone should not be less than 3.5 N/mm^2 for building enclosures (IS: 3620, 1979). Cinder concrete contains cement, sand, and gravel in a 1:2:3 ratio. Cinder concrete replaces 20% of the Portland cement with fly ash (IS: 6042, 1969). Its compressive strength should not be less than 2 N/mm^2. Expanded polystyrene was used as an insulation material between the wall layers. Cement plaster (cement to sand mortar ratio of 1:6) was applied at either side of the wall envelope for all material types.

2.2 Experimental Methodology

Fig. 1 presents images of the building and insulating materials of the wall enclosures considered. In this paper, these materials were used as building enclosure materials for analyzing thermal performance.

Thermal properties such as specific heat capacity and thermal conductivity were measured experimentally using the KD2 Pro thermal properties analyzer (hot wire probe method) (ASTM:D5334-14, 2016). The above equipment can measure thermal conductivity in a range from 0.02 to 2.00 W/mK and volumetric specific heat from 0.5 to 4.0 MJ/m^3K with 10% accuracy. The probe consists of a dual needle (30 mm length, 1.3 mm diameter, and 6 mm spacing). The transient heat source has supplied from an electrical input. One needle acted as a heating source, and the other acted as a monitoring source. The thermophysical properties were obtained from the temperature-time relationship. Two holes were drilled in building materials with the corresponding size so that the probe needle fit tightly into the holes. During the measurement, thermal grease was applied to the dual needle to avoid contact resistance error. The density of the brick was obtained by the ratio between its average mass and volume (IS:2185, 2005). The uncertainty of thermal conductivity, density, and specific heat were calculated for each of all tested building materials (Holman, 2012). The measured thermophysical properties of building materials with uncertainty are presented in Table 1.

Fig. 1. Building and insulation materials of wall enclosures.

Table 1 Thermophysical properties of building wall enclosure materials.

2.3 Thermal analysis:

Seven different wall envelope configurations with four brick materials with either side cement plastered (burnt brick, mud brick, laterite stone, and cinder concrete) and one insulation material (expanded polystyrene) were considered for the investigation of dynamic thermal characteristics. Thermal performance was analyzed under various atmospheric wind velocities. The configurations

Final version is available on: https://doi.org/10.1016/j.envres.2020.110577

investigated include: (1) no insulation (C-H_1), (2) with an insulation layer at the external side (C-H_2), (3) with an insulation layer at the center (C-H_3), (4) with an insulation layer on the internal side (C-H_4), (5) with one insulation layer on the external side and another at the internal side (C-H_5), (6) with one insulation layer at the external side and another at the center (C-H_6), and (7) with one insulation layer at the center and another at the internal side of the envelope (C-H_7). Fig. 2 shows the configurations of the composite wall enclosures and the expanded polystyrene insulation considered.

Fig. 2. Configuration of composite wall enclosures and expanded polystyrene insulation considered in this study.

Information related to the dynamic characteristics of the wall envelopes (as many as 28 combinations of composite walls) was computed and investigated to identify the best wall envelope configuration for reduced cooling loads under various atmospheric wind velocities. The thermal admittance method was employed to compute the dynamic thermal characteristics of the wall envelopes. The admittance procedure uses matrices to simplify the temperature and energy cycles for a composite building fabric enclosure (wall or roof) that is subjected to sinusoidal temperature variations at the sun–air node of the enclosure. The building walls do not generate any internal heat, and their thermal properties are the same in all three directions. The governing diffusion equation for the three dimensions of the wall for temperature $T(x,y,z,t)$ without internal heat generation and the same thermal properties in three dimensions can be written as Eq. (1).

$$\frac{\partial T}{\partial t} = \frac{k}{\rho Cp}\left(\frac{\partial^2 T}{\partial x^2} + \frac{\partial^2 T}{\partial y^2} + \frac{\partial^2 T}{\partial z^2}\right) \qquad (1)$$

Final version is available on: https://doi.org/10.1016/j.envres.2020.110577

The building wall has three dimensions (i.e., length, breadth (thickness), and height). Since the temperature differences along the length (*y*) and height of the wall (*z*) are small, the diffusion equation is reduced to one dimension (i.e., through the thickness (*x*) of the wall). The homogeneous and composite walls are exposed to periodic cyclic variations in temperature with heat flow through the wall enclosure in one direction through the thickness of the wall (i.e., horizontally).

The diffusion equation for heat transfer through the thickness of the wall is presented in Eq. (2) (Davies, 2004).

$$\frac{\partial^2 T(x,t)}{\partial X^2} = \frac{\rho Cp}{k}\frac{\partial T(x,t)}{\partial t} \qquad (2)$$

The periodic solution of the diffusion equation is presented in Eqs. (3) to (7).

$$T(x,t) = Aexp(x/\xi)exp(t/\zeta) \qquad (3)$$

Eq. (3) should satisfy the Fourier equation, which is possible only if $\xi^2=\alpha\zeta$.

Here,

$$\alpha = \frac{k}{\rho Cp} \qquad (3a)$$

$$\zeta = \frac{P}{j2\pi} \qquad (3b)$$

$$\xi = \sqrt{\frac{\alpha P}{j2\pi}} \qquad (3c)$$

Final version is available on: https://doi.org/10.1016/j.envres.2020.110577

$$j = \sqrt{-1} \quad (3d)$$

The periodic solution for a wall enclosure of finite thickness exposed to sinusoidal excitation with a given period can be obtained by imposing boundary conditions. The equation can be obtained as follows,

$$\frac{x}{\xi} = \frac{x}{\pm(\alpha P/j2\pi)^{1/2}} = \pm(1+j)\left(\frac{\pi\rho c_p x^2}{kP}\right)^{1/2} = \pm(1+j)\gamma_1 x \quad (4)$$

where

$$\gamma_1 = \sqrt{\pi\rho c_p/kP} \quad (4a)$$

The temperature can be represented as follows:

$$T(x,t) = [Qsinh(\gamma_1 x + j\gamma_1 x) + Rcosh(\gamma_1 x + j\gamma_1 x)]exp(j2\pi t/P) \quad (5)$$

$$T_{ext} = T_{int}cosh(u+ju) + q_{int}\left(sinh(u+ju)\right)/a \quad (5a)$$

$$q_{ext} = T_{int}\left(sinh(u+ju)\right) \times a + q_{int}cosh(u+ju) \quad (5b)$$

The above equations can be rearranged, as shown in Eq. (6).

$$\begin{bmatrix} T_{ext} \\ q_{ext} \end{bmatrix} = \begin{bmatrix} cosh(u+ju) & \left(sinh(u+ju)\right)/a \\ \left(sinh(u+ju)\right) \times a & cosh(u+ju) \end{bmatrix} \begin{bmatrix} T_{int} \\ q_{int} \end{bmatrix} \quad (6)$$

T_{ext} and q_{ext} are sinusoidally varying temperature and heat flux of complex values, respectively, at the external side of the wall enclosure. The values q_{int} and T_{int} are at the internal side of the wall enclosure.

Here,

$$u = \sqrt{\frac{\pi \rho c_p X^2}{kP}} \tag{6a}$$

$$a = \sqrt{\frac{j2\pi k \rho c_p}{P}} \tag{6b}$$

A homogeneous wall enclosure transmission matrix can be written as Eq. (7),

$$\begin{bmatrix} A_1 + jA_2 & (A_3 + jA_4)/a \\ (-A_4 + jA_3).a & A_1 + jA_2 \end{bmatrix} \tag{7}$$

where

$$A_1 = \cosh(u)\cos(u) \tag{7a}$$

$$A_2 = \sinh(u)\sin(u) \tag{7b}$$

$$A_3 = [\cosh(u)\sin(u) + \sinh(u)\cos(u)]/\sqrt{2} \tag{7c}$$

$$A_4 = [\cosh(u)\sin(u) - \sinh(u)\cos(u)]/\sqrt{2} \tag{7d}$$

The convective heat transfer coefficient at the external surface as per CIBSE standards.

$$h_{sext} = 5.8 + 4.1C_s \text{ (For all wind speeds)} \tag{7e}$$

$$h_{sext} = 16.7\, C_s^{0.5} \text{ (For wind speeds up to 3.5 m/s)} \tag{7f}$$

Final version is available on: https://doi.org/10.1016/j.envres.2020.110577

$$h_{sint} = 2.5\ W/m^2\ K \text{ (For internal surface resistance)} \tag{7g}$$

The homogeneous wall enclosure transmission matrix can be written as Eq. (8)[39],

$$\begin{bmatrix} A_1 + jA_2 & (A_3 + jA_4)/a \\ (-A_4 + jA_3).\,a & A_1 + jA_2 \end{bmatrix} \tag{8}$$

where,

$A_1 = \cosh(u)\cos(u)$,

$A_2 = \sinh(u)\sin(u)$,

$A_3 = [\cosh(u)\sin(u) + \sinh(u)\cos(u)]/\sqrt{2}$,

$A_4 = [\cosh(u)\sin(u) - \sinh(u)\cos(u)]/\sqrt{2}$.

The matrices for internal (R_{sint}) and external (R_{sext}) surface film resistances for the wall enclosure can be written as Eq. (9).

$$E_{sint} = \begin{bmatrix} 1 & -R_{sint} \\ 0 & 1 \end{bmatrix} \text{and} E_{sext} = \begin{bmatrix} 1 & -R_{sext} \\ 0 & 1 \end{bmatrix} \tag{9}$$

The internal and external surface resistances of the building envelope can be computed by Eqs. (10) and (11), respectively.

$$\text{Internal surface resistance,} \quad R_{sint} = \frac{1}{(1.2F_e h_r + h_c)} \tag{10}$$

$$\text{External surface resistance,} \quad R_{sext} = \frac{1}{h_c + F_e h_r} \tag{11}$$

Final version is available on: https://doi.org/10.1016/j.envres.2020.110577

The homogeneous wall enclosure transmission matrix with internal and external surface film resistances can be represented by Eq. (12).

$$\begin{bmatrix} T_{int} \\ q_{int} \end{bmatrix} = \begin{bmatrix} 1 & -R_{sint} \\ 0 & 1 \end{bmatrix} \begin{bmatrix} f_1 & f_2 \\ f_3 & f_1 \end{bmatrix} \begin{bmatrix} 1 & -R_{sext} \\ 0 & 1 \end{bmatrix} \begin{bmatrix} T_{ext} \\ q_{ext} \end{bmatrix} \tag{12}$$

The composite wall enclosure transmission matrix can be written as in Eq. (13),

$$\begin{bmatrix} T_{int} \\ q_{int} \end{bmatrix} = \begin{bmatrix} 1 & -R_{sint} \\ 0 & 1 \end{bmatrix} \begin{bmatrix} f_1 & f_2 \\ f_3 & f_1 \end{bmatrix} \begin{bmatrix} g_1 & g_2 \\ g_3 & g_1 \end{bmatrix} \ldots . \begin{bmatrix} 1 & -R_{sext} \\ 0 & 1 \end{bmatrix} \begin{bmatrix} T_{ext} \\ q_{ext} \end{bmatrix} \tag{13}$$

The walled enclosure layers are represented by f and g.

The building enclosure transmission matrix can be represented, as shown in Eqs. (14) and (15).

$$\begin{bmatrix} T_{int} \\ q_{int} \end{bmatrix} = \begin{bmatrix} E_{11} & E_{12} \\ E_{21} & E_{22} \end{bmatrix} \begin{bmatrix} T_{ext} \\ q_{ext} \end{bmatrix} \tag{14}$$

$$\begin{bmatrix} E_{11} & E_{12} \\ E_{21} & E_{22} \end{bmatrix} = \begin{bmatrix} 1 & -R_{sint} \\ 0 & 1 \end{bmatrix} \begin{bmatrix} A_1 + jA_2 & (A_3 + jA_4)/a \\ (-A_4 + jA_3).a & A_1 + jA_2 \end{bmatrix}_f \begin{bmatrix} A_1 + jA_2 & (A_3 + jA_4)/a \\ (-A_4 + jA_3).a & A_1 + jA_2 \end{bmatrix}_g \cdots \begin{bmatrix} 1 \\ 0 \end{bmatrix} \tag{15}$$

where E_{11}, E_{12}, E_{21}, and E_{22} are the matrix components, which are complex numbers.

2.3.2 Steady Thermal transmittance (*U*)

The thermal transmittance of the wall enclosure is the reciprocal of its thermal resistance. It is the ratio of heat transfer through a building envelope to the difference in temperature across the envelope. A lower the thermal transmittance value of the wall envelope results in higher thermal insulation of the envelope as a steady-state quantity. It is represented in Eq. (17) as

$$\mathrm{U} = \frac{1}{\mathrm{R_{sext}} + \left(\frac{\mathrm{x_1}}{\mathrm{k_1}}\right) + \left(\frac{\mathrm{x_2}}{\mathrm{k_2}}\right) + \mathrm{R_{air}} \ldots + \ldots \mathrm{R_{sint}}} \tag{16}$$

where X_1 and X_2 are the wall layer thicknesses, and k_1 and k_2 are the thermal conductivity values of layer-1 and layer-2, respectively.

2.3.3 Thermal admittance (Y)

The envelope material's capability to absorb heat from the atmosphere and release it back to the same over some time is known as thermal admittance. This indicates the thermal mass of the enclosure. They can be computed by Eq. (18).

$$Y = \left| \left(\frac{q_{int}}{T_{int}} \right)_{T_{ext}=0} \right| = |-E_{11}/E_{12}| \quad (17)$$

2.3.4 Attenuation factor (μ) and its decrement delay (ϕ)

The attenuation factor is the difference between the outside and inside wall enclosure temperature swings. The attenuation factor is inversely proportional to the difference between outside and inside temperature swings. Lower attenuation factor or decrement factor results in higher thermal heat capacity or thermal mass. Decrement lag or Time lag or phase shift is the delay in the heat flow from the outside to the inside of the wall enclosure measured in hours. For thin structures with low thermal capacity values, the value of the attenuation factor is unity, and the value of decrement delay is zero. The attenuation factor decreases while decrement delay increases with increasing thermal capacity for structural materials (Alavez-Ramirez et al., 2014). These values can be determined according to Eq. (19) and (20)

$$\mu = \left| -\frac{1}{UE_{12}} \right| \quad (18)$$

$$\phi = \frac{12}{\pi} arctan \left(\frac{Im(-\frac{1}{UE_{12}})}{Re(-\frac{1}{UE_{12}})} \right) \quad (19)$$

2.3.1 Unsteady transmittance (u_{cyc})

The unsteady transmittance of the wall enclosure is the amount of fluctuating heat gain in the wall envelope. The low value of unsteady transmittance implies the low fluctuating heat gain in the wall envelope. It can be computed by the following Eq. (20):

$$u_{cyc} = \left| -\frac{1}{E_{12}} \right| \qquad (20)$$

Thermal characteristics of the envelopes (i.e., walls and roofs) are unsteady. Above Eq. (16) to Eq. (20) were used to find dynamic thermal characteristics of the wall envelope (Davies, 2004).

A MATLAB program was developed to compute the dynamic thermal quantities of homogeneous and composite wall enclosures exposed to various atmospheric wind velocities. Method validation was carried out for both homogeneous and composite wall envelopes against published CIBSE results. The deviation of the calculated results from the CIBSE values was observed to be less than ±1% for homogeneous envelopes and less than ±2.5% for composite envelopes. Computation of the dynamic thermal quantities of wall enclosures by the admittance method requires thermophysical properties of the wall materials (thermal conductivity, specific heat, and density), the thickness of the wall materials (x), the outside wall surface heat transfer coefficient (h_{sext}), and the inside wall surface heat transfer coefficient (h_{sint}). The thicknesses of the composite walls (multilayer walls) considered in this paper are presented in Fig. 2. The outside wall surface heat transfer coefficient (h_{sext}) depends on the atmospheric wind velocity, while the inside wall surface coefficient (h_{sint}) was considered at standstill wind velocities as per CIBSE standards. The external wall envelopes were exposed to atmospheric wind velocities of 0.0, 0.5, 0.7, 2, 4, 6, 8, and 10 m/s. Table 2 shows the influence of wind velocity on external and internal surface heat transfer coefficients. The above parameters were used as input for the admittance method to obtain dynamic thermal quantities such as admittance, attenuation factor, and decrement delay.

Table 2 Influence of wind velocity on external and internal surface heat transfer coefficients of wall enclosures.

In this paper, we present the dynamic thermal performance of seven composite wall configurations (multilayer walls) of burnt brick, mud brick, laterite stone, and cinder concrete with expanded polystyrene insulation material exposed to eight atmospheric wind speeds (n=28 (7 (configurations/designs) x4 (building materials) = total of 28 combinations of composite walls)). The arrangement of the multilayers is given in Fig. 2. The optimum design of composite walls under severe wind velocity conditions is proposed for reduced cooling costs in buildings.

2.4 Energy Economic Analysis:

2.4.1 Heating degree-hours and cooling degree-hours

Heating degree-hours and cooling degree-hours are used to calculate the energy required for heating and cooling of the building. The base temperature is the point at which the mechanical system should be switched on to provide thermal comfort inside the environment. As per the ASHRAE standard, the minimum base temperature is considered to be 23.3 °C for cooling and heating of the built environment. The energy needed for cooling or heating depends upon the difference between the outside temperature and base temperature. The sol air temperature depends upon absorptivity and solar radiation on the building surface, which is considered based on the outside temperature. Cooling degree-hours or days are calculated by the summing the hours or days when the outside sol air temperature is above the base temperature. Similarly, heating degree-hours or days are the sum of the difference between the outside sol air temperature and the base temperature over a particular period of hours or days. ASHRAE metrological data have been used for cooling and heating degree-hours in Chennai climatic conditions (13.0827^{0}N, 80.2707^{0}E). Chennai is located in a hot and humid climatic zone of India. The annual

Final version is available on: https://doi.org/10.1016/j.envres.2020.110577

degree days and hours of Chennai has been presented in Fig. 3. Chennai has only cooling degree days/cooling degree hours, and this climate does not have heating degree days or heating degree hours. Therefore, air-conditioning costs associated with building cooling are significant in this climatic zone.

Fig. 3. Monthly heating and cooling degree days and hours of Chennai (13.0827^{0}N, 80.2707^{0}E).

The total number of cooling degree-days or hours (CDD or CDH) and heating degree-days or hours (HDD or HDH) can be calculated using Eqs. (21-24)

$$CDD = \sum_{l=1}^{N_{CD}} (T_{SO} - T_{ba}) = N_{CD}.\Delta T, \text{ for } T_{so} \geq T_{ba} \quad (21)$$

$$CDH = \sum_{l=1}^{N_{CH}} (T_{SO} - T_{ba}) = N_{CH}.\Delta T, \text{ for } T_{so} \geq T_{ba} \quad (22)$$

$$HDD = \sum_{l=1}^{N_{HD}} (T_{SO} - T_{ba}) = N_{HD}.\Delta T, \text{ for } T_{so} \geq T_{ba} \quad (23)$$

$$HDH = \sum_{l=1}^{N_{HH}} (T_{SO} - T_{ba}) = N_{HH}.\Delta T, \text{ for } T_{so} \geq T_{ba} \quad (24)$$

Where, N_{CD} N_{CH}, $N_{HD,}$ and N_{HH} are the number of cooling days, number of cooling hours, number of heating days, and number of heating hours, respectively. T_{so} is the sol air temperature, and it depends on the outside air temperature, surface absorption, and solar radiation on the surface.

2.4.2 Building material cost and annual energy cost savings

Final version is available on: https://doi.org/10.1016/j.envres.2020.110577

Table 3 shows the building material costs of various building materials with their dimensions. The mud brick is the cheapest building material among all four building materials studied. The thermo-economic method was proposed by Duffie et al. (1985). Annual energy-cost savings is the yearly cooling cost savings obtained when using insulation. It can be calculated using Eq. (25). Table 4 shows the parameters used for the energy economic analysis to obtain annual energy cost savings, life cycle saving costs, and payback periods.

$$\text{ESC} = \frac{10^{-3} E.CDH.\Delta u_{cyc}}{COP} \tag{25}$$

Where Δu_{cyc} is the difference in unsteady thermal transmittance with and without insulation.

Table 3 Building material cost of various building materials.

Table 4 Parameters used for energy-economic analysis.

2.4.3 Life cycle cost savings

Life cycle cost savings is the total energy savings throughout the lifetime calculated by including the insulation cost and building material cost. It can be calculated using Eq. (26).

$$\text{LCS} = \frac{10^{-3}.P_1.E.CDH.\Delta u_{cyc}}{COP} - C_{inv} \tag{26}$$

Present worth factor (P_1) depends upon the inflation rate (f), discount rate (D), and life cycle period of building materials (N). It can be calculated using Eq. (27). Investment cost (C_{inv}) is the sum of insulation cost (C_{ins}) and building material cost (C_{bm}).

$$P_1 = \frac{1}{D-f}\left[1-\left(\frac{1+f}{1+D}\right)^N\right] \quad (27)$$

2.4.4 Payback period

Payback period refers to the time (usually in years) that it takes to recover the initial investment of insulation cost and building material cost. It can be calculated using Eq. (28)

$$PB = \frac{C_{inv}}{ESC} \quad (28)$$

3. Results and Discussion

3.1. Unsteady transmittance and admittance of various wall designs and wall materials

The steady transmittance (U) is not accurate measure of thermal performance as it takes only thermal conductivity property in calculations under steady state conditions as in Eq. (16). In practice, the properties (Specific heat capacity and density) contributing to thermal mass should also be considered under periodic heat transfer conditions for the computation of accurate unsteady thermal transmittance (u_{cyc}) and air-conditioning cost savings as presented in Eqs. (20) & (25). The findings of both higher admittance values and lower unsteady transmittance values imply the reduced heat fluctuation gain in the building. Fig. 4 (a) shows the unsteady transmittance and admittance of composite burnt brick wall enclosures exposed to various external heat transfer coefficients. The configurations that save the most energy from a higher admittance (lower unsteady transmittance) perspective across all seven studied configurations at all external surface heat transfer coefficients and wind velocities are the burnt brick composite wall envelope with an expanded polystyrene insulation layer positioned at the center of the burnt brick envelope (C-H_3) and the burnt brick composite wall envelope with one part of the expanded polystyrene insulation layer positioned at the external side, and another positioned at the center (C-H_6). At 10 m/s external wind velocity, the burnt brick composite wall envelope with an expanded polystyrene insulation layer positioned at the center of the burnt brick envelope (C-H_3) has an admittance value of 4.898 W/m^2K and an unsteady transmittance value of 0.39W/m^2K. At 10 m/s external wind velocity, the burnt brick composite wall enclosure with one part of the expanded polystyrene insulation layer positioned at the external side and another positioned at the center (C-H_6) had an admittance value of 4.779 W/m^2K and an unsteady transmittance value of 0.21W/m^2K. The burnt brick composite wall envelope without an insulation layer (C-H_1) had admittance and unsteady transmittance values of 4.5744 W/m^2K and 1.21 W/m^2K, respectively. For any building wall, high thermal admittance indicates high thermal mass and low unsteady thermal transmittance, leading to high thermal storage. Among all seven studied configurations, C-H_3 and C-H_6 are preferable at all external surface heat transfer coefficients/wind velocities due to the high admittance values at low unsteady transmittance.

Fig. 4 (b) presents the unsteady transmittance and admittance of composite mudbrick wall enclosures exposed to various external heat transfer coefficients. C-H_3 and C-H_6 are the most energy-saving configurations at all external surface heat transfer coefficients and wind velocities from a higher admittance (lower unsteady transmittance) perspective among the seven studied configurations. At 10 m/s external wind velocity, C-H_6 has a 4.6798 W/m^2K admittance value and a 0.29 W/m^2K unsteady transmittance value. In contrast, C-H_1 has a 4.4832 W/m^2K admittance value and a 1.26 W/m^2K unsteady transmittance value.

Fig. 4 (c) shows the unsteady transmittance and admittance of composite laterite wall enclosures at all external surface heat transfer coefficients and wind velocities. C-H_3 and C-H_6 configurations provide the most energy savings from a higher admittance (lower unsteady transmittance) perspective among the seven studied configurations at all external wind velocities. At 10 m/s external wind velocity, C-H_3 has

Final version is available on: https://doi.org/10.1016/j.envres.2020.110577

an admittance value of 5.3902 W/m^{2}K and a 0.41 W/m^{2}K unsteady transmittance value, while C-H_6 has a 5.2664 W/m^{2}K admittance value and an unsteady transmittance value of 0.20 W/m^{2}K. C-H_1 has admittance and unsteady transmittance values of 5.0247 W/m^{2}K and 1.64 W/m^{2}K, respectively.

Fig. 4 (d) presents the unsteady transmittance and admittance of composite cinder concrete wall enclosures. C-H_3 and C-H_6 configurations provide most energy savings from a higher admittance (lower unsteady transmittance) perspective for all the external surface heat transfer coefficients and wind velocities among the seven studied configurations. At 10 m/s external wind velocity, C-H_3 has an admittance value of 4.4929 W/m^{2}K and an unsteady transmittance value of 0.39 W/m^{2}K, while C-H_6 has admittance and unsteady transmittance values of 4.3812 W/m^{2}K and 0.21 W/m^{2}K, respectively. C-H_1 has an admittance value of 4.1905 W/m^{2}K and an unsteady transmittance value of 1.15 W/m^{2}K.

For any building wall, higher thermal admittance indicates a higher thermal mass, while lower unsteady thermal transmittance indicates higher thermal insulation. Among the seven configurations, C-H_3 and C-H_6 are preferable for all external surface heat transfer coefficients and wind speeds due to the higher admittance values at lower unsteady transmittance.

Fig. 4. Unsteady transmittance and admittance of composite wall enclosures for various external surface heat transfer coefficients: (a) burnt brick, (b) mudbrick, (c) laterite stone, and (d) cinder concrete.

3.2 Attenuation factor and decrement delay of various wall designs and wall materials

Fig. 5(a) shows the attenuation factor of composite burnt brick wall enclosures at various external surface heat transfer coefficients. C-H_5 and C-H_6 provide the most energy savings from a lower attenuation factor point of view at all external wind velocities and across all seven studied configurations. At 10 m/s external wind velocity, C-H_5 has the lowest attenuation factor of 0.1896, and C-H_6 has a low attenuation factor of 0.2041. C-H_1 has the highest attenuation factor value of 0.5172. Fig. 5(b) shows the decrement delay of composite burnt brick wall enclosures at various external surface heat transfer coefficients. C-H_5 and C-H_7 provide the most energy savings with a higher decrement delay at all external wind velocities across all seven studied configurations. At a 10 m/s external wind velocity, C-H_5 has the highest decrement delay of 9.9059 h, and C-H_7 also has a high decrement delay of 8.9944 h. C-H_1 has the lowest decrement delay value of 6.4079 h.

Fig. 5. (a) Attenuation factor, and (b) decrement delay of composite burnt brick wall enclosures at various external surface heat transfer coefficients.

Fig. 6(a) presents the attenuation factor of composite mudbrick wall enclosures for various external surface heat transfer coefficients. C-H_5 and C-H_6 provide the most energy-savings from a lower attenuation factor point of view across all seven configurations at all external wind velocities. At 10 m/s external wind velocity, C-H_5 has the lowest attenuation factor of 0.1965, and C-H_6 also has a low attenuation factor of 0.2147. C-H_1 has the highest attenuation factor value of 0.5219.

Fig. 6(b) presents the decrement delay of composite mudbrick wall enclosures at various external surface heat transfer coefficients. C-H_5 and C-H_7 configurations provided the most energy savings from a higher decrement lag perspective across the seven configurations and at all external wind velocities. At 10 m/s external wind velocity, C-H_5 has the highest decrement lag of 9.8365 h, and C-H_7 also has a high decrement lag of 8.955 h. C-H_1 has the lowest decrement delay value of 6.4245 h.

Fig. 6. (a) Attenuation factor, and (b) decrement delay of composite mudbrick wall enclosures at various external surface heat transfer coefficients.

Final version is available on: https://doi.org/10.1016/j.envres.2020.110577

Fig. 7(a) shows the attenuation factor of composite laterite wall enclosures at various external surface heat transfer coefficients. C-H_5 and C-H_6 provided the most energy savings from a lower attenuation factor point of view across all seven studied configurations and at all external wind velocities. At 10 m/s external wind velocity, C-H_5 has the lowest attenuation factor of 0.1737 due to a higher thermal mass offered by the insulation position. C-H_6 also has a low attenuation factor of 0.1738. C-H_1 has the highest attenuation factor value of 0.5364 because of the lower thermal mass of the wall.

Fig. 7(b) shows the decrement delay of composite laterite wall enclosures at various external surface heat transfer coefficients. C-H_5 and C-H_7 provide the most energy savings from a higher decrement lag perspective across the seven studied configurations and at all external wind velocities. At 10 m/s external wind velocity, C-H_5 has the highest decrement lag of 9.7889 h, and C-H_7 also has a high decrement lag of 8.7059 h. C-H_1 has the lowest decrement lag value of 5.8129 h.

Fig. 7. (a) Attenuation factor, and (b) Decrement delay of composite laterite wall enclosures at various external surface heat transfer coefficients.

Fig. 8 (a) shows the attenuation factor of composite cinder concrete walls at various external surface heat transfer coefficients. C-H_5 and C-H_6 provide the most energy savings with the lowest attenuation factor among the seven studied configurations at all external wind velocities. At 10 m/s external wind velocity, C-H_5 has the lowest attenuation factor of 0.2544, and C-H_6 also has a low attenuation factor of 0.2941. C-H_1 has the highest attenuation factor value of 0.6044.

Fig. 8(b) shows the decrement delay of composite cinder concrete walls at various external surface heat transfer coefficients. C-H_5 and C-H_7 provide the most energy savings with a higher decrement lag across all seven studied configurations at all external wind velocities. At 10 m/s external wind velocity, C-H_5 has the highest decrement lag of 8.857 h, and C-H_7 also has a high decrement lag of 8.0459 h. C-H_1 has the lowest decrement delay value of 5.6926 h.

Final version is available on: https://doi.org/10.1016/j.envres.2020.110577

Fig. 8. (a) Attenuation factor, and (b) decrement delay of composite cinder concrete wall enclosures at various external surface heat transfer coefficients.

3.3. Annual energy cost savings and life cycle cost savings of various wall designs and wall materials

Fig. 9 shows that the life cycle cost savings dependent upon the position of the insulation and quantity of insulation material. Because the quantity of insulation material is constant for the designs of C-H_2 to C-H_7, the cost of insulation should be maintained consistently in all those configurations. The brunt brick with expanded polystyrene and the resulting six configurations (e.g., from C-H_2 to C-H_7) show annual energy cost savings of 1.18, 1.03, 1.03, 1.25, 1.22, and 1.15 \$/m^2, respectively. Among all configurations studied, C-H_5 shows the highest annual energy cost savings for the four different materials (i.e., burnt brick, mud brick, laterite stone, and cinder concrete with expanded polystyrene) of 1.25, 1.20, 1.71, and 1.29 \$/m^2, respectively. The C-H_5 configuration also shows the highest life cycle cost savings for the burnt brick, mud brick, laterite stone, and cinder concrete expanded polystyrene as 10.95, 11.16, 18.32, and 11.62 \$/m^2, respectively. Among all the configuration studied, C-H_5 is found as the best performer for all building materials.

Fig. 9. Impact of configuration on insulation cost and life cycle cost savings.

Fig. 10 shows that the increase in the wind velocity or external heat transfer coefficient for the configuration (C-H_5) leads to an increase in annual energy cost savings and life cycle cost savings. As the wind velocity increased from 0 to 10m/s, there is increase in the annual energy cost savings of burnt brick, mud brick, laterite stone and cinder concrete with expanded polystyrene in the order 103%

Final version is available on: https://doi.org/10.1016/j.envres.2020.110577

(increase from 0.72 to 1.46 \$/m^2), 98% (increase from 0.70 to 1.38 \$/m^2), 133% (increase from 0.9 to 2.09 \$/m^2) and 84% (increase from 0.81 to 1.47 \$/m^2), respectively. At 2 m/s wind speed, the burnt brick, mud brick, laterite stone, and cinder concrete recorded the annual energy cost savings of 1.25, 1.20, 1.71, and 1.29 \$/m^2, respectively. As the wind velocity increased from 0 to 10 m/s, there is increase in the life cycle cost savings of burnt brick, mud brick, laterite stone, and cinder concrete with expanded polystyrene in the order of 345% (from 3.16 to 14.11 \$/m^2), 264% (from 3.79 to 13.80 \$/m^2), 277% (from 6.35 to 23.97 \$/m^2) and 218% (from 4.49 to 14.28 \$/m^2), respectively. The increase in the annual energy cost savings and life cycle cost savings is significant in the wind speed range 0 to 2 m/s. In contrast, the increase in the values of annual energy cost savings and life cycle cost savings is gradual in the wind speed range 2 m/s to 10 m/s. At 2 m/s wind speed, the burnt brick, mud brick, laterite stone, and cinder concrete have life cycle cost savings of 10.95, 11.16, 18.32, and 11.62 \$/m^2, respectively. Among all building materials studied, the laterite with expanded polystyrene and configuration (C-H_5) showed the highest life cycle cost savings and the highest annual energy cost savings at every wind speed.

Fig. 10. Annual energy cost savings and life cycle cost savings of various wall designs.

Fig. 11 shows building, insulation, energy saving, and life cycle saving costs of CH-5 wall enclosure at 2 m/s external wind velocity. The recommended order for the highest energy cost savings is laterite, cinder concrete, burnt brick, and mud brick. The life cycle cost saving considers both energy cost savings and investment costs of building materials. The recommended order for the highest life cycle saving costs is laterite stone, cinder concrete, mud brick, and burnt brick. The mud brick shows better life cycle costs than burnt brick due to its lowest investment cost.

Fig. 11. Building, insulation, energy saving, and life cycle saving costs of CH-5 wall enclosure at 2 m/s external wind velocity.

3.4 Payback periods of various wall designs and wall materials

Fig. 12 shows that the increase in wind velocity leads to a reduction in the payback period. As the wind velocity increased from 0 to 10 m/s, the reductions in the payback period of burnt brick, mud brick, laterite, and cinder concrete with expanded polystyrene are 50.63% (reduction from 10.37 to 5.12 years), 49.0% (reduction from 9.2 to 4.77 years), 57.1% (reduction from 7.67 to 3.3 year), and 45.11% (reduction from 9.4 to 5.04 years), respectively. At 2 m/s wind speed, the burnt brick, mud brick, laterite stone, and cinder concrete have payback periods of 6, 5.48, 4.03, and 5.74 years, respectively. Among all building materials studied, the laterite stone with expanded polystyrene has the lowest payback period at all wind speeds.

Fig. 12. Payback periods of building materials.

4. Conclusions

In this paper, we considered seven different types of cost-effective external wall designs relevant to the manufacture of dwellings in emerging economies. Specifically, we studied the effect of surface external heat transfer coefficients on thermal performance characteristics of the walls and their air-conditioning cost-savings potential. Four different types of building materials with expanded polystyrene insulation were considered with seven different outer enclosure configurations. The main conclusions of the study are:

- C-H_5 (with one insulation layer at the external side and another at the internal) is the best wall envelope design configuration because it provides a lower attenuation factor, as well as highest decrement lag values at all wind velocities among the seven, studied wall enclosure designs. Hence, this wall enclosure design is the best to reduce heat gain by convection.

- The variable with the greatest effect on outer building enclosure performance is the material used. The laterite with $C\text{-}H_5$ enclosure design offers the highest annual energy cost savings (1.71 $/m^2 at 2 m/s), highest life cycle cost savings (18.32 $/m^2 at 2m/s) and the lowest payback period (4.03 year at 2 m/s) at all wind speeds as compared to the other studied building materials. The preference order of building materials for high net annual cost savings and low payback periods is found as: laterite stone > cinder concrete > mud brick >burnt brick.
- A study of the thermal performance parameters is essential for non-air-conditioned buildings, whereas the study of annual energy cost savings, life cycle costs, and payback periods are essential for air-conditioned buildings. The preference order of the wall designs for improved thermal performance parameters in non-air-conditioned buildings is $C\text{-}H_5 > C\text{-}H_6 > C\text{-}H_2 > C\text{-}H_7 > C\text{-}H_4 > C\text{-}H_3 > C\text{-}H_1$, and this order applies very well to air-conditioned buildings as well.
- The most significant changes in the thermal performance characteristics, life cycle cost savings, annual energy cost savings, and payback periods occur between wind speeds of 0 and 2 m/s. Above 2 m/s wind speed, the changes in thermal performance characteristics and energy economic parameters are gradual.

The results of the work will help inform the development of energy-conscious yet cost-effective buildings in emerging economies.

Acknowledgements

Final version is available on: https://doi.org/10.1016/j.envres.2020.110577

KHK acknowledges the support made by a grant from the National Research Foundation of Korea (NRF) funded by the Ministry of Science, ICT & Future Planning (Grant No: 2016R1E1A1A01940995).

Nomenclature			
C_{bm}	Building material cost ($/m²)	P	Time period [s]
C_{ins}	Insulation cost ($/m²)	P_1	Present worth factor
C_{inv}	Investment cost ($/m²)	q_{ext}	External heat flux of complex values at x=0 [W/m²]
Cp	Specific heat [J/kgK]	q_{int}	Internal heat flux of complex values at x=X [W/m²]
Cs	Wind speed [m/s]	R_{air}	Air resistance [m²K/W]
D	Discount rate [%]	R_{sint}	Internal surface resistance [m²K/W]
E	Electricity price ($/kWh)	R_{sext}	External surface resistance [m²K/W]
E_{11}, E_{12}, E_{21}, E_{22}	Elements of composite wall transmission matrix	t	Time [s]
f	Inflation rate (%)	T_b	Base temperature [°C]
f_1, f_2, f_3, f_4	Elements of homogeneous wall matrix	T_{ext}	External temperature variation [°C]
Fe	Emissivity factor[-]	T_{int}	Internal temperature variation [°C]
g_1, g_2, g_3, g_4	Elements of homogeneous wall matrix	T_{so}	sol air temperature [°C]
hc	Convective heat transfer coefficient [W/m² K]	u_{cyc}	Cyclic transmittance [W/m²K]
hr	Radiative heat transfer coefficient [W/m² K]	U	Thermal transmittance [W/m²K]
h_{sext}	External surface heat transfer coefficient [W/m² K]	R_t	Thermal resistance with insulation [m²K/W]
h_{sint}	Internal surface heat transfer coefficient [W/m² K]	X	Thickness of the wall [m]
k	Thermal Conductivity [W/mK]	x	Finite thickness [m]
K	Geometry constant	Y	Admittance [W/m²K]
l	Insulation thickness (m)		
Greek symbols			

α	Thermal diffusivity [m^2/s]	ρ	density [kg/m^3]
ε	Emissivity of the wall [-]	σ	Boltzmann constant [5.67 X 10^{-8} $W/m^2 K^4$]
μ	Attenuation factor [-]	ϕ	Decrement lag [h]
Abbreviations			
BB	Burnt brick	HDD	Heating degree days
CNC	Cinder concrete	HDH	Heating degree-hours
COP	Coefficient of performance	LS	Laterite stone
CDD	Cooling degree days	LSC	Life cycle saving cost
CDH	cooling degree-hours	MB	Mud-brick
EP	Expanded polystyrene	P	Cement plaster
ESC	Annual energy saving cost	PB	Payback period

References

Alavez-Ramirez, R., Chiñas-Castillo, F., Morales-Dominguez, V., Ortiz-Guzman, M., Lara-Romero, J., 2014. Thermal lag and decrement factor of a coconut-ferrocement roofing system. Constr. Build. Mater. 55, 246–256. https://doi.org/10.1016/j.conbuildmat.2014.01.048

Antonopoulos, K.A., Koronaki, E.P., 2000. Effect of indoor mass on the time constant and thermal delay of buildings. Int. J. Energy Res. 24, 391–402. https://doi.org/10.1002/(SICI)1099-114X(200004)24:5<391::AID-ER585>3.0.CO;2-L

Arslan, O., Ozgur, M.A., Yildizay, H.D., Kose, R., 2010. Fuel effects on optimum insulation thickness: An exergitic approach. Energy Sources, Part A Recover. Util. Environ. Eff. 32, 128–147. https://doi.org/10.1080/15567030903196327

Asan, H., S.Y.., 1998. Effects of Wall's thermophysical properties on time lag and decrement factor. Energy Build. 28, 159–166. https://doi.org/10.1016/s0378-7788(98)00030-9

ASHRAE, 2001. American Society of Heating, Refrigerating and air-conditioning engineers,Chapter 30 Fenestration. Atlanta. https://doi.org/10.1016/0038-092X(83)90020-8

ASTM:D5334-14, 2016. Standard Test Method for Determination of Thermal Conductivity of Soil and Soft Rock by Thermal Needle Probe Procedure 04, 6–13. https://doi.org/10.1520/D5334-0814.2

Balaji, N.C., Mani, M., Venkatarama Reddy, B. V., 2019. Dynamic thermal performance of conventional and alternative building wall envelopes. J. Build. Eng. 21, 373–395. https://doi.org/10.1016/j.jobe.2018.11.002

Baniassadi, A., Sajadi, B., Amidpour, M., Noori, N., 2016. Economic optimization of PCM and insulation layer thickness in residential buildings. Sustain. Energy Technol. Assessments 14, 92–99. https://doi.org/10.1016/j.seta.2016.01.008

CIBSE, 2006. CIBSE Environmental Design Guide A. The Chartered Institution of; Building Services Engineers London. https://doi.org/10.4324/9781315671796

Davies, M., 2004. Building Heat Transfer. John Wiley & Sons Ltd,.

Duffie, J.A., Beckman, W.A., McGowan, J., 1985. Solar Engineering of Thermal Processes, American Journal of Physics. https://doi.org/10.1119/1.14178

Duffin, R.J., 1984. A passive wall design to minimize building temperature swings. Sol Energy 33, 337–342.

Evola, G., Marletta, L., 2013. A dynamic parameter to describe the thermal response of buildings to radiant heat gains. Energy Build. 65, 448–457. https://doi.org/10.1016/j.enbuild.2013.06.026

Feng, W., Huang, J., Lv, H., Guo, D., Huang, Z., 2018. Determination of the economical insulation thickness of building envelopes simultaneously in energy-saving renovation of existing residential buildings. Energy Sources, Part A Recover. Util. Environ. Eff. 41, 665–

676. https://doi.org/10.1080/15567036.2018.1520349

Gagliano, A., Patania, F., Nocera, F., Ferlito, A., Galesi, A., 2012. Thermal performance of ventilated roofs during summer period. Energy Build. 49, 611–618. https://doi.org/10.1016/j.enbuild.2012.03.007

Gülten, A., 2020. Determination of optimum insulation thickness using the entransy based thermoeconomic and environmental analysis: a case study for Turkey. Energy Sources, Part A Recover. Util. Environ. Eff. 42, 219–232. https://doi.org/10.1080/15567036.2019.1649330

Hall, M., Allinson, D., 2008. Assessing the moisture-content-dependent parameters of stabilised earth materials using the cyclic-response admittance method. Energy Build. 40, 2044–2051. https://doi.org/10.1016/j.enbuild.2008.05.009

Hall M R, 2010. Materials for energy efficiency and thermal comfort in buildings, CRC Press,U.K. https://doi.org/10.1017/CBO9781107415324.004

Holman, J.P., 2012. Experimental Methods for Engineers. McGraw-Hill Companies.

Huang, J., Lv, H., Feng, W., Qu, P., Huang, Z., 2020. Determination of economical thermal insulation thickness for a building wall with two parallel structures. Energy Sources, Part A Recover. Util. Environ. Eff. 42, 399–409. https://doi.org/10.1080/15567036.2019.1587086

IS: 1725, 1982. Specification for soil based blocks used in general building constructuion. Indian Stand. institution, New Delhi, India 13.

IS: 2117, 2002. Indian standard guide for manufacture of hand-made common burnt clay building bricks. Indian Stand. institution, New Delhi, India.

IS: 3620, 1979. Indian standard specification for laterite stone block for masonry. Indian Stand. institution, New Delhi, India.

IS: 6042, 1969. Indian standard code of practice for construction of lightweight concrete block masonry. Indian Stand. institution, New Delhi, India.

IS:2185, 2005. Concrete Masonry Units — Specification, Part 1 Hollow and Solid Concrete Blocks.

Kontoleon, K.J., Eumorfopoulou, E.A., 2008. The influence of wall orientation and exterior surface solar absorptivity on time lag and decrement factor in the Greek region. Renew. Energy 33, 1652–1664. https://doi.org/10.1016/j.renene.2007.09.008

Kontoleon, K.J., Theodosiou, T.G., Tsikaloudaki, K.G., 2013. The influence of concrete density and conductivity on walls' thermal inertia parameters under a variety of masonry and insulation placements. Appl. Energy 112, 325–337. https://doi.org/10.1016/j.apenergy.2013.06.029

Kumar, K.., Saboor, S., Kumar, V., Kim, K.H., Babu T. P., A., 2018. Experimental and theoretical studies of various solar control window glasses for the reduction of cooling and heating loads in buildings across different climatic regions. Energy Build. 173, 326–336. https://doi.org/10.1016/j.enbuild.2018.05.054

Lee Ok, K., Medina, M.A., Raith, E., Sun, X., 2014. Assessing the integration of a thin phase change material (PCM) layer in a residential building wall for heat transfer reduction and management q. Appl. Energy.

Mavromatidis, L.E., EL Mankibi, M., Michel, P., Santamouris, M., 2012. Numerical estimation of time lags and decrement factors for wall complexes including Multilayer Thermal Insulation, in two different climatic zones. Appl. Energy 92, 480–491. https://doi.org/10.1016/j.apenergy.2011.10.007

Najim, K.B., 2014. External load-bearing walls configuration of residential buildings in Iraq and their thermal performance and dynamic thermal behaviour. Energy Build. 84, 169–181. https://doi.org/10.1016/j.enbuild.2014.07.064

Najim, K.B., Fadhil, O.T., 2015. Assessing and improving the thermal performance of reinforced concrete-based roofing systems in Iraq. Energy Build. 89, 213–221. https://doi.org/10.1016/j.enbuild.2014.12.049

Ng, S.C., Low, K.S., Tioh, N.H., 2011. Thermal inertia of newspaper sandwiched aerated lightweight concrete wall panels: Experimental study. Energy Build. 43, 2956–2960. https://doi.org/10.1016/j.enbuild.2011.06.022

Ozel, M., Pihtili, K., 2007. Optimum location and distribution of insulation layers on building walls with various orientations. Build. Environ. 42, 3051–3059. https://doi.org/10.1016/j.buildenv.2006.07.025

Ruivo, C.R., Ferreira, P.M., Vaz, D.C., 2013. On the error of calculation of heat gains through walls by methods using constant decrement factor and time lag values. Energy Build. 60, 252–261. https://doi.org/10.1016/j.enbuild.2013.02.001

Shaik, S., Talanki, A.B.P.S., 2016. Optimizing the position of insulating materials in flat roofs exposed to sunshine to gain minimum heat into buildings under periodic heat transfer conditions. Environ. Sci. Pollut. Res. 23, 9334–9344. https://doi.org/10.1007/s11356-015-5316-7

Shaik, S., Talanki Puttaranga Setty, A.B., 2016. Influence of ambient air relative humidity and temperature on thermal properties and unsteady thermal response characteristics of laterite wall houses. Build. Environ. 99, 170–183. https://doi.org/10.1016/j.buildenv.2016.01.030

Ulgen, K., 2002. Experimental and theoretical investigation of effects of wall's thermophysical properties on time lag and decrement factor. Energy Build. 34, 273–278.

https://doi.org/10.1016/S0378-7788(01)00087-1

Yu, J., Yang, C., Tian, L., Liao, D., 2009. A study on optimum insulation thicknesses of external walls in hot summer and cold winter zone of China. Appl. Energy 86, 2520–2529. https://doi.org/10.1016/j.apenergy.2009.03.010

List of figures

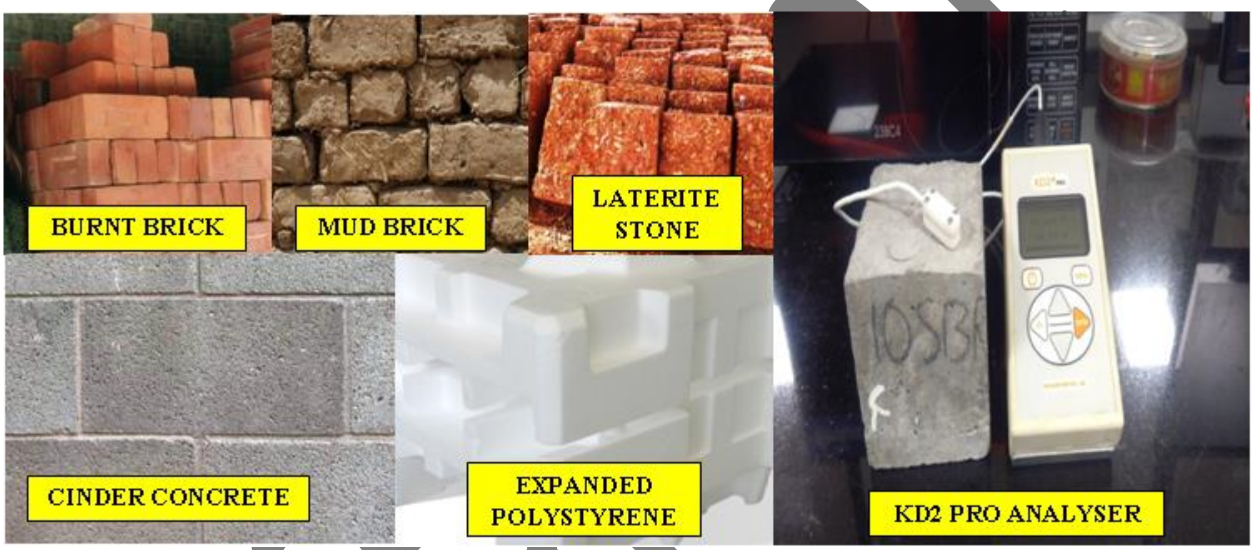

Fig. 1. Building and insulation materials of wall enclosures.

Final version is available on: https://doi.org/10.1016/j.envres.2020.110577

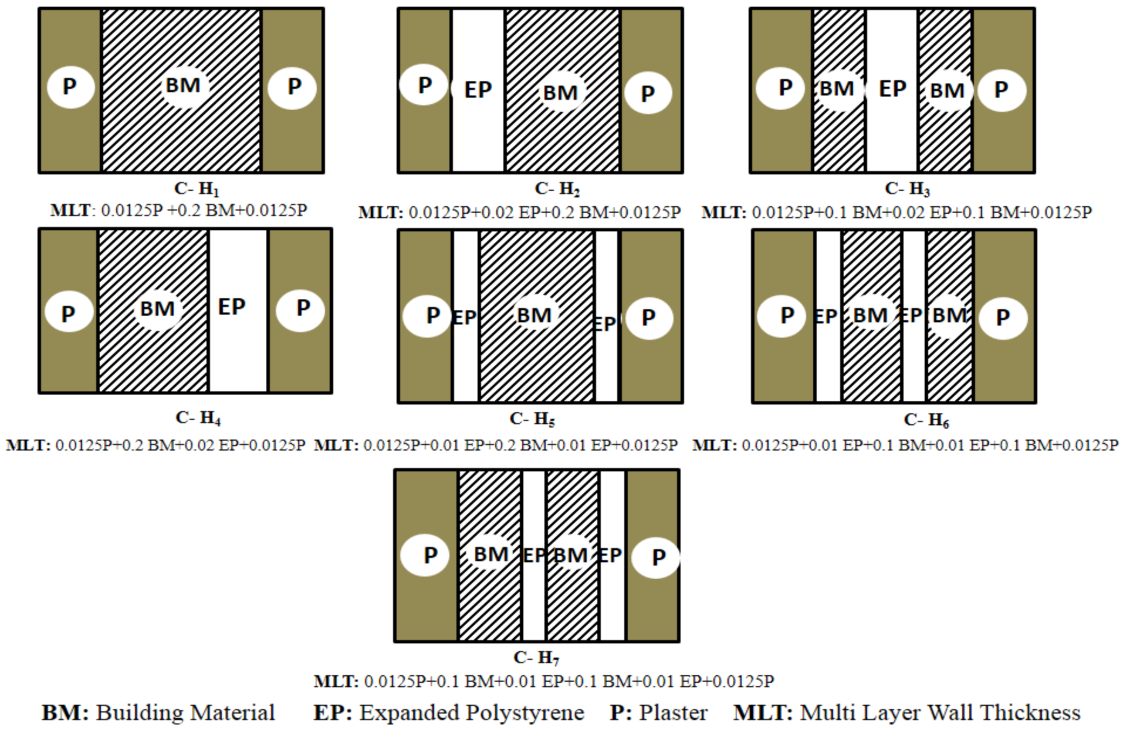

Fig. 2. Configuration of composite wall enclosures and expanded polystyrene insulation considered in this study.

Final version is available on: https://doi.org/10.1016/j.envres.2020.110577

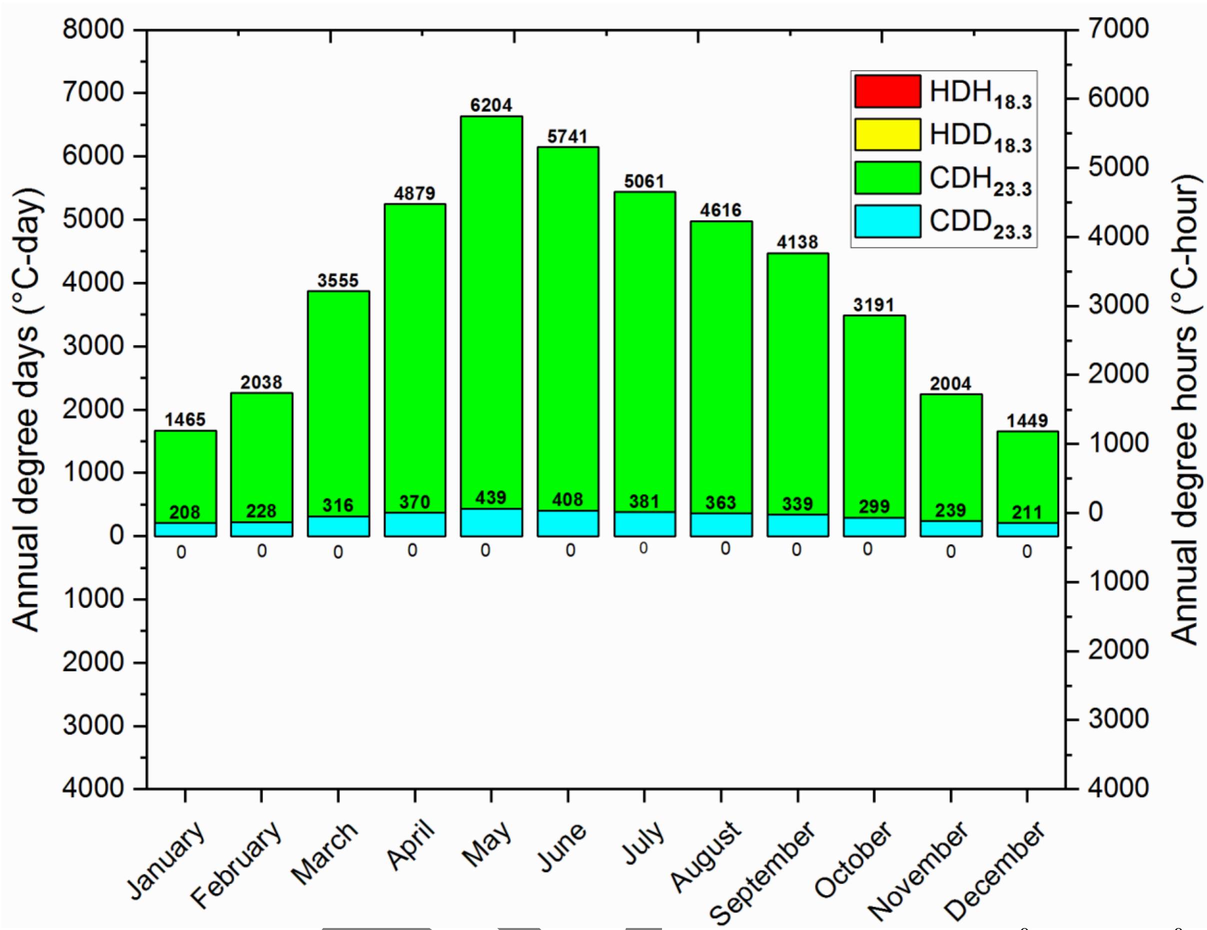

Fig. 3. Monthly heating and cooling degree days and hours of Chennai (13.0827^{0}N, 80.2707^{0}E).

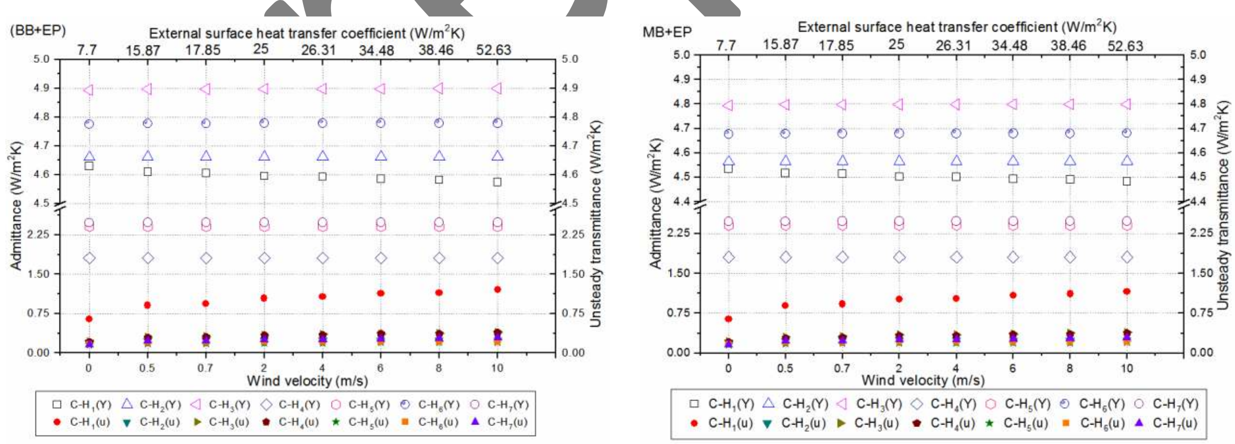

(a) (b)

Final version is available on: https://doi.org/10.1016/j.envres.2020.110577

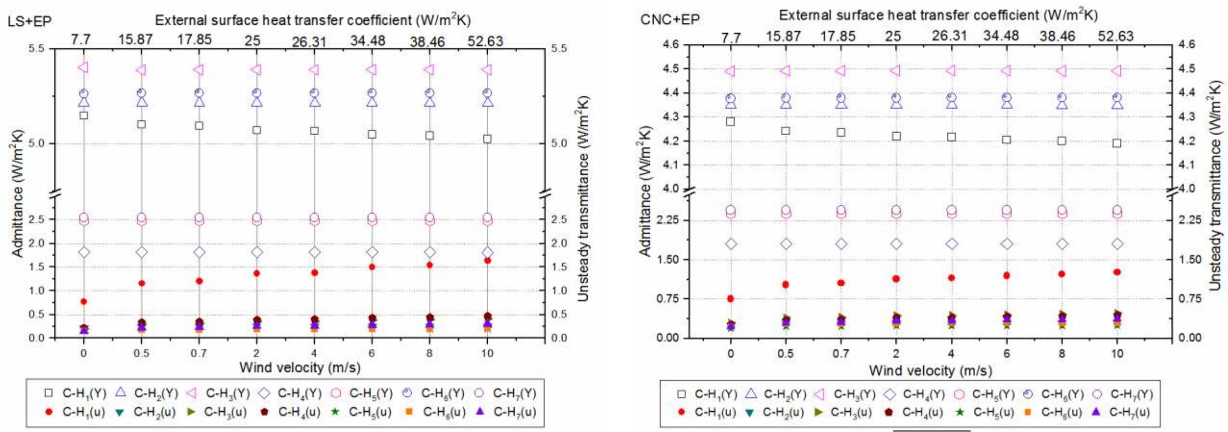

(c) (d)

Fig. 4. Unsteady transmittance and admittance of composite wall enclosures for various external surface heat transfer coefficients: (a) burnt brick, (b) mudbrick, (c) laterite stone, and (d) cinder concrete.

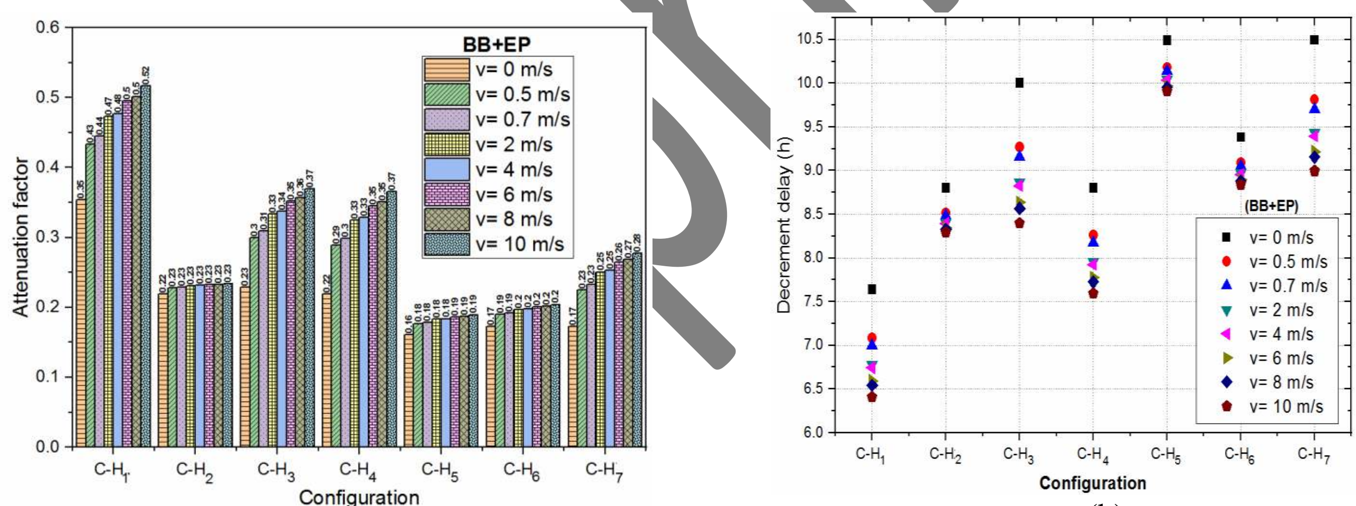

(a) (b)

Fig. 5. (a) Attenuation factor, and (b) decrement delay of composite burnt brick wall enclosures at various external surface heat transfer coefficients.

Final version is available on: https://doi.org/10.1016/j.envres.2020.110577

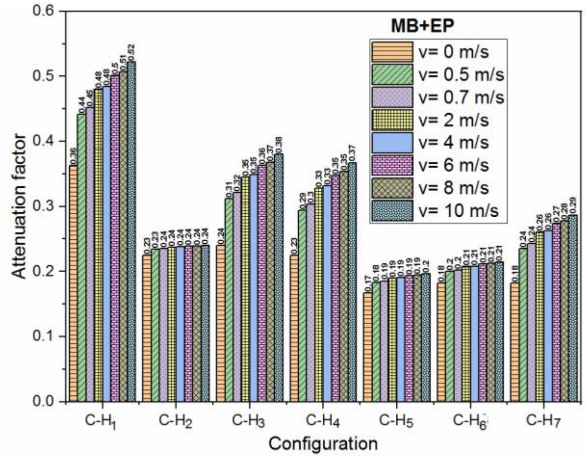

(a)

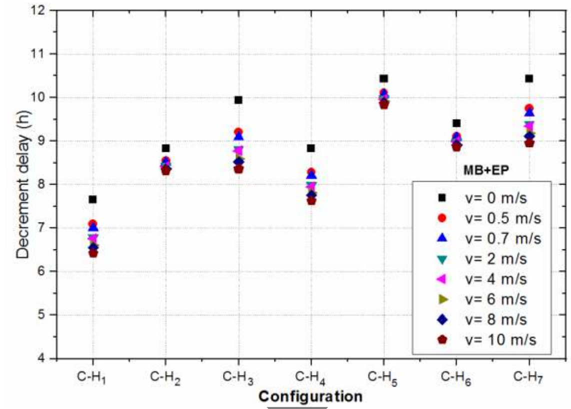

(b)

Fig. 6. (a) Attenuation factor, and (b) decrement delay of composite mudbrick wall enclosures at various external surface heat transfer coefficients.

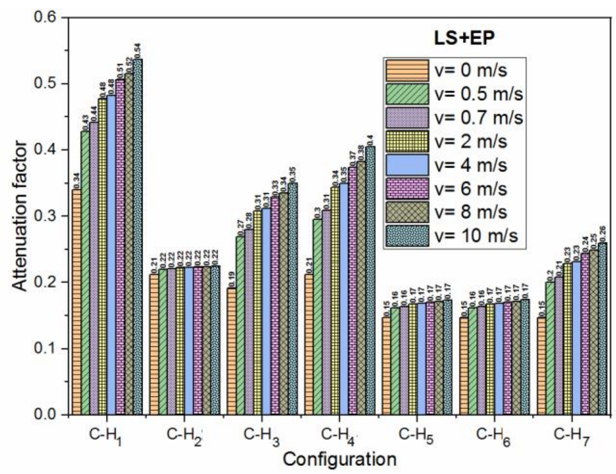

(a)

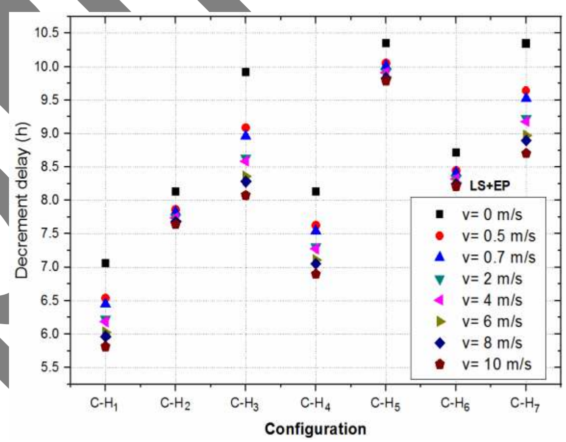

(b)

Fig. 7. (a) Attenuation factor, and (b) Decrement delay of composite laterite wall enclosures at various external surface heat transfer coefficients.

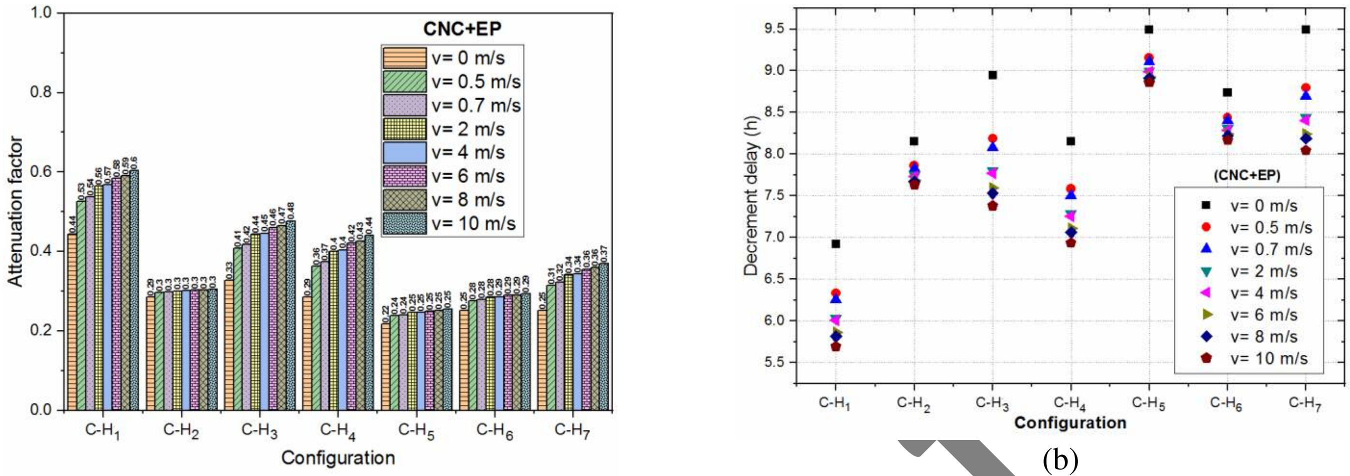

(a) (b)

Fig. 8. (a) Attenuation factor, and (b) decrement delay of composite cinder concrete wall enclosures at various external surface heat transfer coefficients.

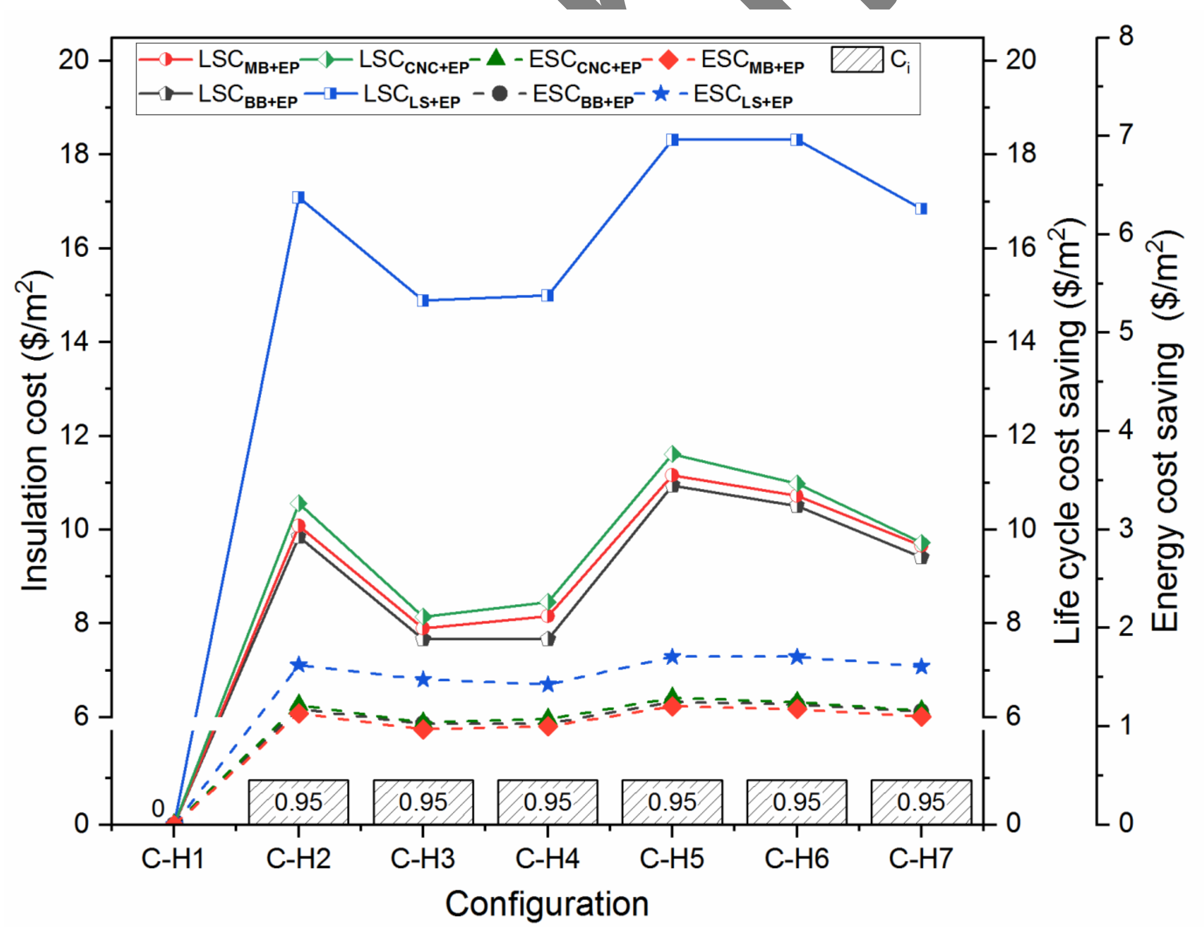

Fig. 9. Impact of configuration on insulation cost and life cycle cost savings.

Final version is available on: https://doi.org/10.1016/j.envres.2020.110577

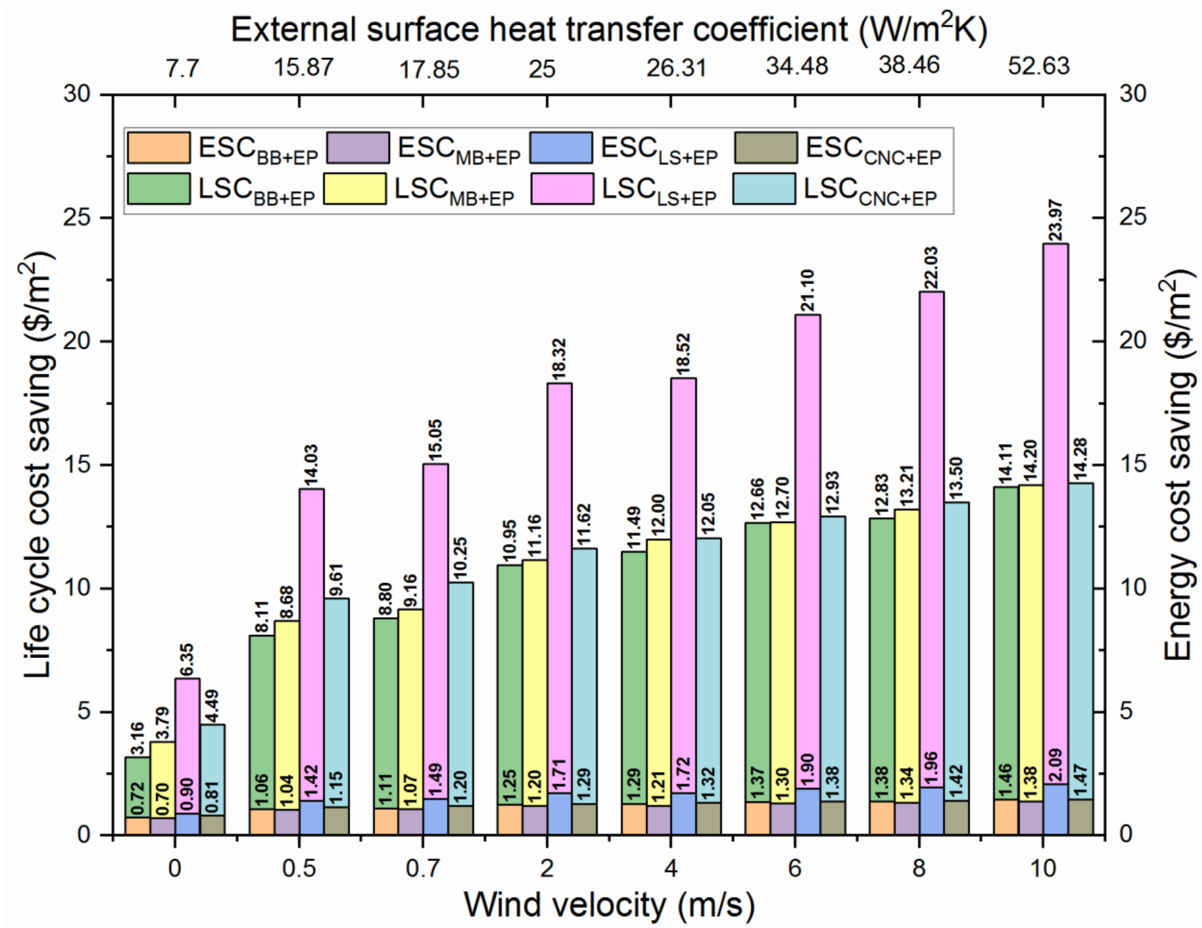

Fig. 10. Annual energy cost savings and life cycle cost savings of various wall designs.

Final version is available on: https://doi.org/10.1016/j.envres.2020.110577

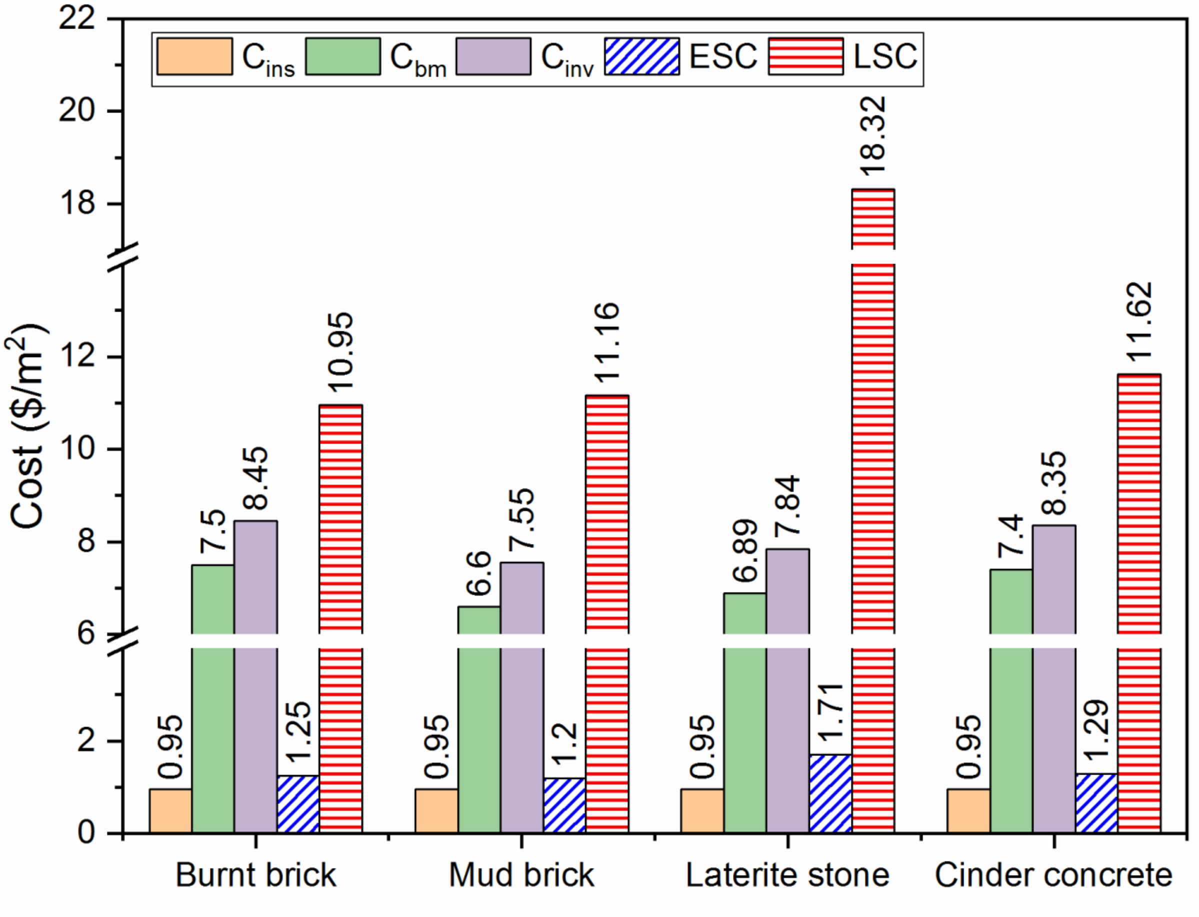

Fig. 11. Building, insulation, energy, and life cycle saving costs of CH-5 wall enclosure at 2 m/s external wind velocity.

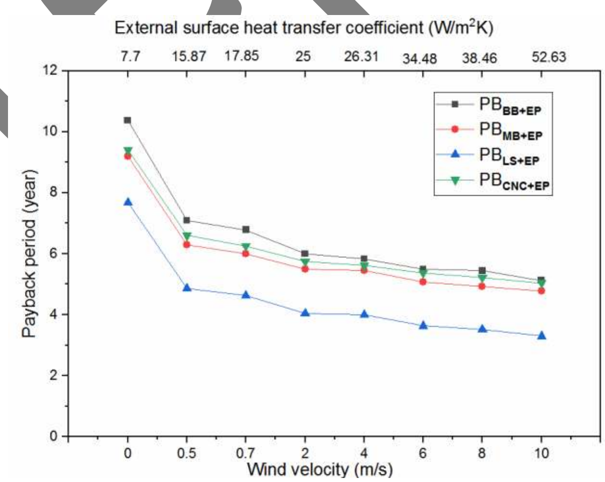

Fig. 12. Payback periods of building materials.

Final version is available on: https://doi.org/10.1016/j.envres.2020.110577

List of tables

Table 1 Thermophysical properties of building wall enclosure materials.

S. No.	Building material	Code	Thermal conductivity k [W/mK]	Density ρ [kg/m^3]	Specific heat C_p [J/kgK]
1.	Burnt brick	BB	0.811±0.003	1820±7	880±0.02
2.	Mudbrick	MB	0.75±0.002	1731±6	880±0.01
3.	Laterite stone	LS	1.369±0.004	1000±4	1926±0.04
4.	Cinder concrete	CNC	0.686±0.003	1406±3	840±0.03
5.	Expanded polystyrene	EP	0.038±0.001	16±1	1340±0.05
6.	Cement plaster	P	0.721±0.002	1762±2	840±0.02

Table 2 Influence of wind velocity on external and internal surface heat transfer coefficients of wall enclosures.

S. No.	Atmospheric wind velocity at the outer side of the wall enclosure [m/s]	External surface heat transfer coefficient $h_{sext}=\frac{1}{R_{sext}}$ [W/m^{2}K]
1.	Standstill	7.70
2.	0.5	15.87
3.	0.7	17.85
4.	2	25.00
5.	4	26.31
6.	6	34.48
7.	8	38.46
8.	10	52.63

Table 3 Building material cost of various building materials

S. No.	Building materials	Dimensions (m) (LBH)	No. of brick required /m^2	\$/m^2
1.	Burnt brick	0.23 x 0.101 x 0.076	108	7.5
2.	Mud brick	0.23 x 0.101 x 0.076	108	6.6
3.	Laterite stone	0.305 x 0.2 x 0.2	15	6.89

4.	Cinder concrete	0.41 x 0.2 x 0.2	11	7.4

Table 4 Parameters used for energy-economic analysis.

S. No.	Parameter	Value
1.	Cooling degree-hours (CDH)	44343 ^{o}C- h
2.	Heating degree-hours (HDH)	0
3.	Unit cost of electricity (E)	0.082 $/kWh (Kumar et al., 2018)
4.	Discount rate (D)	6.25%
5.	Inflation rate (f)	3.44%
6.	Insulation thickness (l)	0.02 m
7.	Insulation cost (C_{ins})	0.95 $/m^2
8.	Coefficient of performance (COP)	2.5 (Kumar et al., 2018)
9.	Life cycle period of building materials (N)	20 (Yu et al., 2009)
10.	Present worth factor (P_1)	14.77